Numerical simulation of nozzle flow field with jet vane thrust vector control

M S R C Murty[1], **M S Rao**[2], and **D Chakraborty**[1]*
[1]Directorate of Computational Dynamics, Defence Research and Development Laboratory, Hyderabad, India
[2]Directorate of Propulsion, Defence Research and Development Laboratory, Hyderabad, India

The manuscript was received on 17 August 2009 and was accepted after revision for publication on 14 October 2009.

DOI: 10.1243/09544100JAERO677

Abstract: Numerical simulations are performed to characterize the jet vane thrust vector control mounted in the rear of a rocket motor. The three-dimensional Navier–Stokes equations along with the K–ε turbulence model are solved in a hybrid mesh consisting of an unstructured grid and a structured grid. All essential flow features including the complex compression/expansion wave interactions emanating from the vane surfaces and shrouds are captured by simulation. The computed side force coefficients are seen to vary linearly with chamber pressure and vane deflection angles. A theoretical correlation has been developed by a non-linear regression analysis from the computational fluid dynamics (CFD) database to predict the force and moment coefficients for different chamber pressures, vane deflection angle, and roll offset angle. The theoretical correlation compare very well with full CFD simulation as well as the experimental data.

Keywords: jet vane, thrust vector control, regression analysis, computational fluid dynamics

1 INTRODUCTION

At low flight speeds when aerodynamic surfaces can generate only weak control force, control and stability requirements of smaller vehicles can be achieved by thrust vector control (TVC) systems. The TVC system provides the necessary lateral forces for quick change of the flight path by reorienting the direction of thrust vector. Thrust vector control can be achieved with secondary injection of gas/liquid into the nozzle gas flow, the flex nozzle, jet vane, jet tabs, and many others [**1**]. Jet vanes are used on small solid rocket motors due to advantages such as low actuation torque, small installation envelope, and quick response capability to control pitch, yaw, and roll simultaneously [**2–4**]. The basic principle of obtaining control forces by jet vanes is explained in reference [**5**].

If the mechanical and chemical erosion of the vanes caused by the hot rocket exhaust is neglected, vanes provide the control forces just like supersonic wings providing lift at an angle of attack in the free stream. The schematic of the supersonic flow around a two-dimensional (2D) profile is shown in Fig. 1.

When the vane is deflected at a typical angle to exhaust gas, the windward side experiences increased surface pressure due to shock and the expansion caused decreases surface pressure in the leeward side. This difference of pressure in the windward and leeward sides of the vane provides a force normal to the chord of the vane. The side force component of the normal force is used to control the missile and drag component results in thrust loss. The smaller the ratio of thrust loss to the side force the better the performance of the jet vane. To characterize the jet vane system it is necessary to calculate the forces and moments as accurately as possible. If the jet vanes are placed at the rear end of the nozzle without any shroud, shock wave theory can be applied to calculate the aerodynamic forces and moments. In the presence of the shroud, the shock waves generated by the vanes impinge on the shroud wall and increase the pressure. The complex shock wave interaction present in the vane and shroud region is very difficult to predict with semi-empirical formulae. Moreover, in case of vanes with X-formation, all four vanes operate so that the required control force is achieved and the relative position of each vane affects the additional force on the shroud wall.

*Corresponding author: Directorate of Computational Dynamics, Defence Research and Development Laboratory, Kanchanbagh P.O., Hyderabad 500058, India.
email: debasis_cfd@drdl.drdo.in; debasis_drdl@yahoo.co.in*

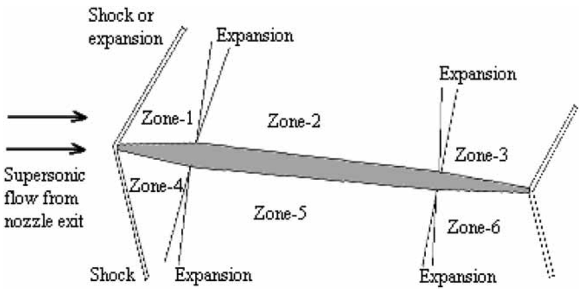

Fig. 1 Typical shock structure for supersonic flow past jet vane-type geometry

In practice, the jet vanes are exposed to the hot exhaust gas of the rocket nozzle with temperatures as high as 3000 K and velocities up to Mach 3.5 that exert severe thermal and mechanical loads on jet vane. Due to reaction with the combusted gases, vane surfaces are ablated chemically and mechanically at different rates depending on the combusted gas composition, convective heat transfer rate on a surface, and the vane material. The erosion in the vane at high temperature and velocities is very difficult to predict [**6**]. As the vane surface area gets reduced with time due to erosion, the magnitude of side force generated by the vane reduces and directly affects its ability to control the vehicle. Due to complexity of modelling erosion, the characterization of jet vanes is usually done through an experimental [**7**, **8**] and a semi-empirical [**9**] method, and a combination of numerical, semi-empirical, experimental methods [**5**].

The literature on numerical simulation of the jet vane is very limited. Roger *et al.* [**2**] have numerically studied the flow field in the vicinity of the jet vane mounted at the exit of the nozzle using an Upwind Flux Difference Splitting Navier–Stokes solver along with the Baldwin Lomax turbulence model [**10**] or a compressible two equation K–ε turbulence model [**11**], and obtained reasonable good agreement for the forces and moments with the static test results. Saha *et al.* [**12**] simulated the jet vane flow field in the cold flow wind tunnel test condition as well as in the presence of hot rocket exhaust. While the vane characteristics match extremely well with cold flow condition in the wind tunnel test, the erosion of the vane in the presence of hot exhaust affected the aerodynamic performance of the vane and proper modelling of Jet vane erosion was stressed. Yu *et al.* [**13–15**] studied the surface ablation and thermal response analysis of the jet vane surface by coupling computational fluid dynamics (CFD) Solver Fluent and an integral form of thermal boundary layer equations; the predicted vane surface temperature match reasonably well with the experimental results. Sung and Hwang [**5**] studied the fluid dynamics interference of the TVC shroud on the aerodynamics performance of the jet vanes arranged in X-formation within the shroud. The predicted side force coefficient from an integrated method consisting of a semi-empirical model, 3D numerical analysis, and static firing tests of full-scale motor match reasonably well with the experimental results.

In this present work, the performance of the jet vane TVC system of an aerospace vehicle is evaluated numerically for different duty cycle combinations in ground test condition. In the present case, a tungsten-based alloy is taken for jet vanes so that erosion is likely to be minimal during the jet vane operation. A theoretical correlation based on the CFD database is developed to predict the vane characteristics (side force and rolling moment) for a given chamber pressure and a vane deflection angle. The results obtained from the theoretical correlation are compared with the CFD and experimental results.

2 EXPERIMENTAL CONDITION FOR WHICH SIMULATIONS ARE CARRIED OUT

For developing a flight-worthy jet vane thrust vector control system, extensive ground testing is required. In the present case, four jet vanes in X-formation is mounted at the exit of a rocket motor. The schematic of the test configuration is shown in Fig. 2. All dimensions are normalized with respect to the rocket nozzle exit diameter. The measurement of the forces and moments are carried out according to a predefined duty cycle in a six-component static test. All the four vanes are deflected by different angles as presented in

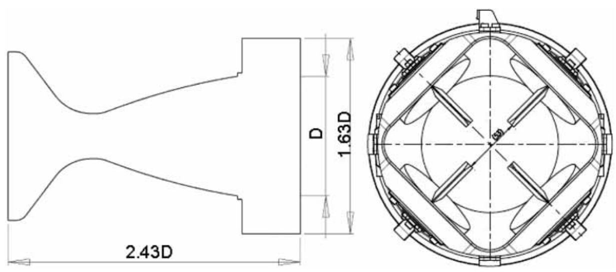

Fig. 2 Arrangement of jet vanes at the exit of the nozzle

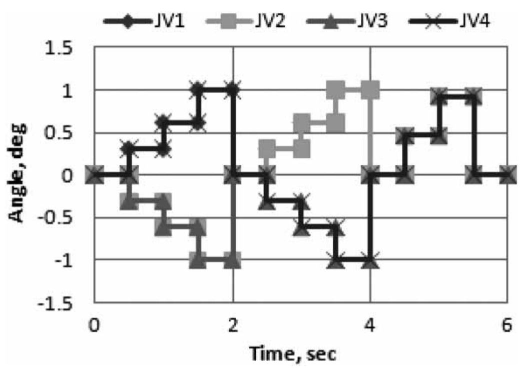

Fig. 3 Normalized vane deflection history of four jet vanes

Fig. 3. The vane deflection is normalized by the maximum deflection value. The stagnation temperature of the rocket motor exhaust gas is 2944 K and the stagnation pressure varies between 95 and 130 ksc during the motor operation.

3 COMPUTATIONAL METHODOLOGY

Simulations are carried out using a commercial CFD software. It solves a 3D Navier–Stokes equation in an unstructured, hybrid grid system using a collocated variable arrangement. To simulate high Mach number compressible flow (as in the present case), a density band solver is used along with Roe Flux Difference Splitting Scheme [**16**] for spatial discretization and first-order implicit Euler Scheme for temporal discretization. Turbulence is modelled using the K–ε turbulence model along with wall function.

4 RESULTS AND DISCUSSION

4.1 Description of flow field

A number of numerical simulations are carried out with different chamber pressures and different vane deflection angles. The schematic of computational domain is shown in Fig. 4. It consists of a CD nozzle, a TVC module, and a free stream region covering exhaust plume up to the length of 48 exit diameters of the nozzle. In the simulation, the X-axis is taken along the longitudinal direction, whereas the Y- and Z-axis are taken along the height and width, as shown in the Fig. 4. The origin is taken at the centre of the nozzle exit plane.

In the nozzle inlet plane, stagnation temperature and stagnation pressures are specified and the atmospheric conditions are specified at far field, outflow, and the rest of the inflow domain. A hybrid grid consisting of an unstructured grid in the jet vane assembly and a multi-block structured hexahedral grid in the remaining portion of the flow field is employed. A typical grid distribution in the computational domain is shown in Fig. 5. In the jet vane and shroud assembly,

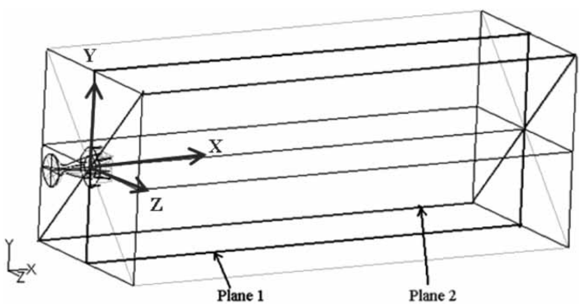

Fig. 4 Coordinate system and computational domain (Plane 1: passes in between jet vanes. Plane 2: passes through the jet vane)

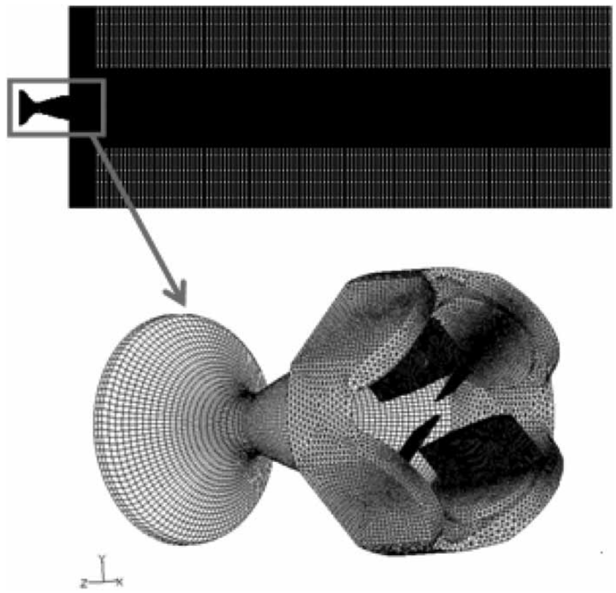

Fig. 5 Computational grid in the jet vane flow field

unstructured grid is generated, and the rest of the flow field consists of a multi-block structured hexahedral grid. The grid is very fine in the jet vane region and in the central portion of the computational domain to capture the complex jet structure. Different meshing iterations have been performed to arrive at a suitable distance for the first grid point near the wall, to obtain the required y^+ value ($\sim$65) for good solution.

Grid independence of the solution is studied by comparing the solution with three different grids namely 0.412, 1.735, and 3.145 million cells in the domain. The computed side force coefficients for 16° vane deflection with three different grids are presented in Table 1, it is observed that by changing the grid from 1.735 million to 3.145 million, there is very little change in the computed side force, thus demonstrating the gird independence of the results. Side force coefficients are obtained by normalizing the force with free stream dynamic pressure and vehicle cross-sectional area.

Both first- and second-order spatial discretization were attempted. Although the second-order schemes captured the flow features more crisply, the computed side force and the drag force differ marginally between first- and second-order discretization schemes. The computed side forces are 132 and 135 Kgf for the first-order scheme and the second-order scheme, respectively, giving a maximum difference of 2.5 per cent.

Table 1 Comparison of side force with different grids

Grid No.	Size (in million)	Side force coefficient
Grid-1	0.412	1.197
Grid-2	1.735	1.259
Grid-3	3.145	1.261

Further simulations were carried out with the first-order discretization scheme. The qualitative features of the flow field are depicted through Mach number contour (Fig. 6) in the symmetry plane for different vane deflections in the pitch plane namely 0°, 8°, 16°, and 26°. With an increase in the deflection angle, the plume structure gets distorted more and more.

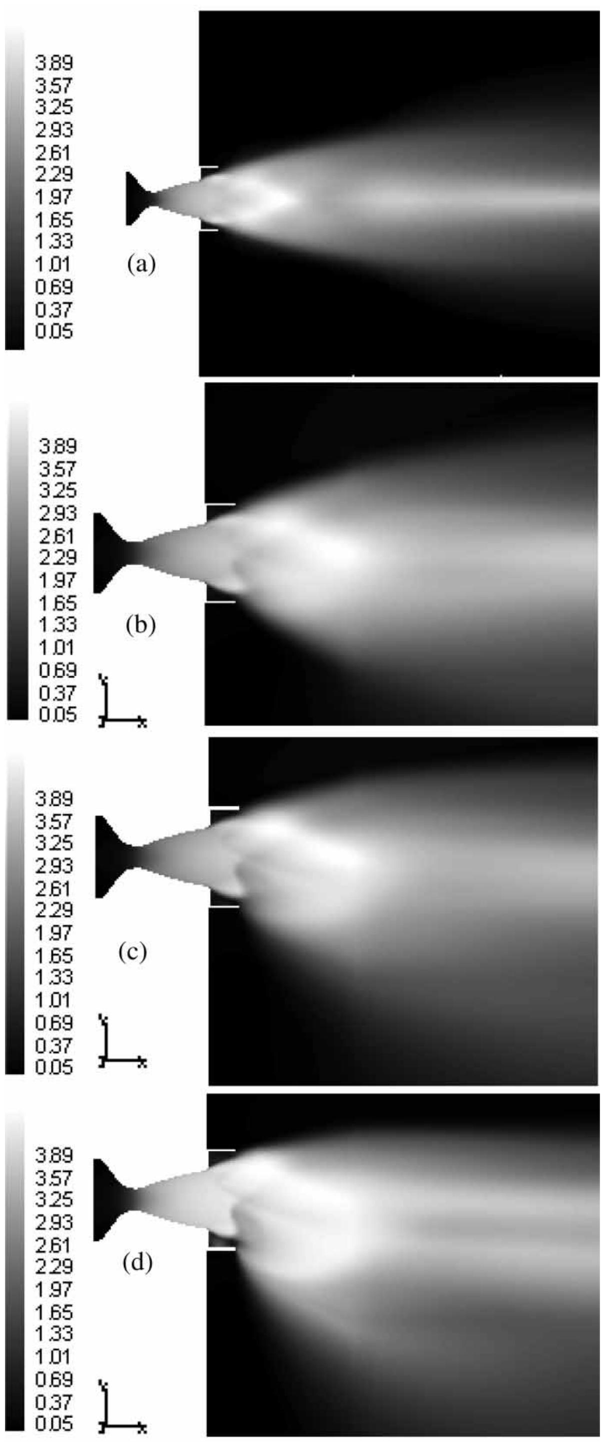

Fig. 6 Mach no. distribution in the pitch plane with different vane deflections: (a) 0°; (b) 8°; (c) 16°; and (d) 26°

The blown-up view of the pressure field around the jet vane area is shown in Fig. 7. The pressure fields around the deflected and undeflected vanes are also shown in the figure. It can be seen that

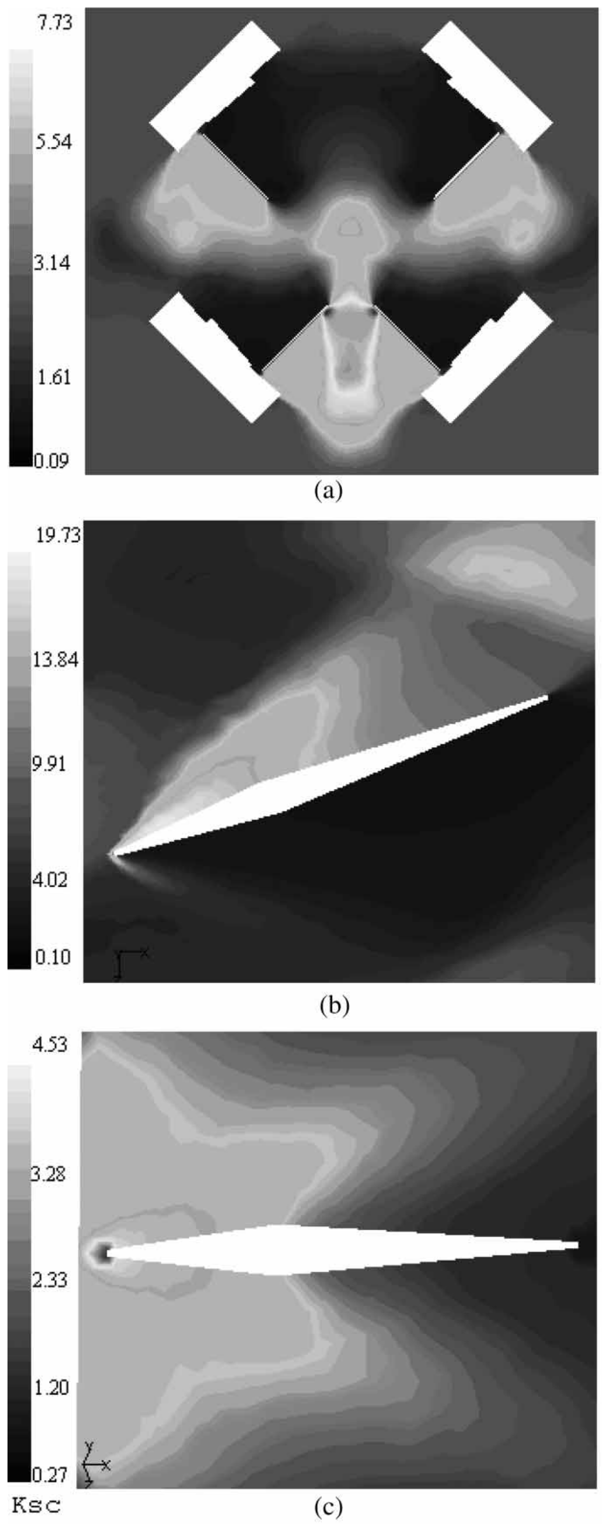

Fig. 7 Blown-up view of the pressure distribution around the jet vane: (a) near the shroud; (b) around the deflected vane at 26°; and (c) around the un-deflected vane

the compression waves emanating from the vanes is hitting the vane shroud and giving rise to a complex shock reflection pattern, as discussed previously. The pressure fields around the vanes in the deflected and undeflected positions are markedly different.

In the undeflected position, both windward and leeward surfaces experience similar pressure, whereas in the defected position, the windward surface pressure is significantly more than the leeward surface pressure. The computed surface pressure field for the windward and leeward sides of the vane of two deflection angles 8° and 26° is shown in Fig. 8. The windward side of the vane experiences compression, whereas the leeward surface experiences expansion. The difference of the surface pressure in the windward and leeward sides generates required pitch and yaw force of the vane.

The magnitude of surface pressure in the windward direction increases with the increase in the vane deflection. Variations of pitch force and yaw force

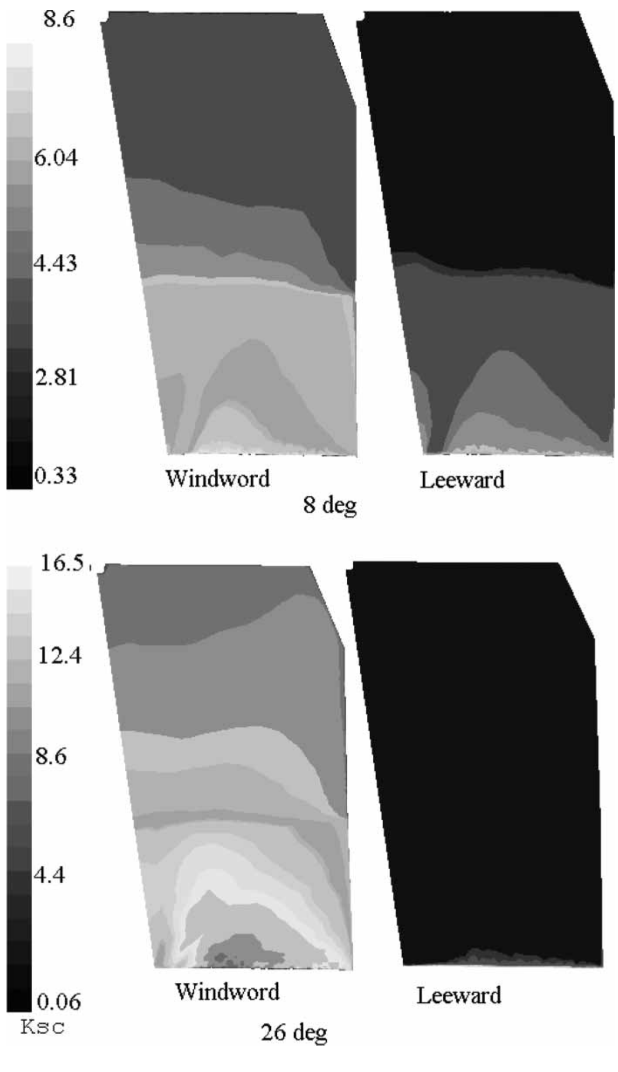

Fig. 8 Surface pressure comparison between the windward and leeward sides of the vane with different vane deflection angles: (a) 8° and (b) 26°

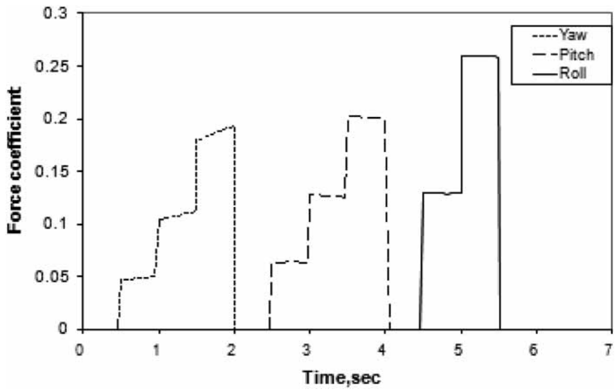

Fig. 9 Variation of computed yaw, pitch, and roll forces with deflection angle

coefficients generated by the TVC system with various deflection angles are presented in Fig. 9. The force coefficient C_F $(= F/q \cdot s)$ is obtained by normalizing the force with free stream dynamic pressure (q) and vehicle cross-section area (s). To facilitate the design of an actuator, hinge moment is calculated at the centre of pressure for various vane deflection angles. The non-dimensional hinge moment coefficient is presented in Fig. 10 for various vane deflections (vane length is used as the length scale for a moment coefficient). A hinge moment coefficient changes from a positive to a negative value with an increase in the deflection angle.

4.2 Correlation development

Characterization of the TVC system involves many parameters, namely chamber pressure, jet vane angles, rotational offset angles, and their combination. Performing CFD simulation or doing the ground test for all different combinations is impractical. Moreover, the vehicle mission control may require dynamically changing side forces/roll moments to suit its trajectory. Development of theoretical correlation is very much beneficial for the characterization of jet

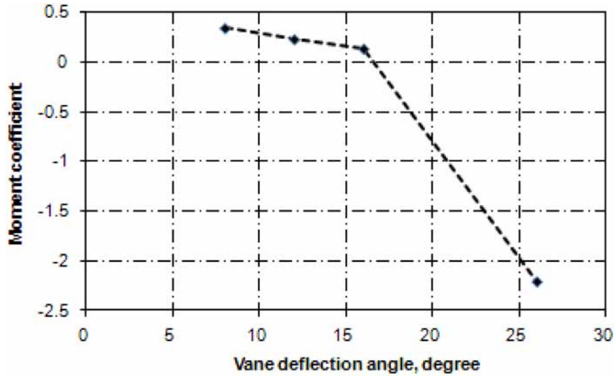

Fig. 10 Variation of hinge moment coefficient with vane deflection angle

vane systems. The effect of chamber pressure and vane angles on the generated side force is explored through number of numerical simulations by varying the parameters. The variation of a side force coefficient with chamber pressure and vane angles are presented in Fig. 11. Side force coefficient is seen to vary linearly with both chamber pressure and jet vane angles. Such a linear relationship facilitates development of a simpler correlation.

The CFD database is generated for different chamber pressures and vane angles and the resultant force and moments are tabulated for each condition. A theoretical model is developed by performing non-linear regression analysis to predict the side force/roll moment for any combination of chamber pressure, jet vane angle, and rotational offset angle. A random 3D equation generator was used to find the best equation that fits the data well. Regression analysis software 'Table Curve 3D 4.0' and 'DataFit 8.1.69' have been used for the study. Although many fits are possible, a simple non-linear model $Y = \mathrm{X1} * \mathrm{X2}/a$ ($a = 5.815\,05$) with standard error 2.7337 is used for the present analysis. The coefficient of multiple determinations (R^2), which measures the proportion of variation in data points, is 0.999 712 9, indicating a very good fit. A rotational offset angle is included in the model to take care of roll orientation of the vehicle. Figure 12 shows the sign convention for a vehicle rotation offset angle.

The right-hand screw rule is used for the sign convention of jet vane deflection, when the thumb point towards the hinge location. The following equations are solved to obtain pitch, yaw, and roll force coefficients. In the offset co-ordinate, the forces are given by

$$F^1_{\mathrm{Y,Z,R}} = \frac{P_{\mathrm{C}}(\xi_1 \times \delta_1 + \xi_2 \times \delta_2 + \xi_3 \times \delta_3 + \xi_4 \times \delta_4)}{A} \tag{1}$$

The net yaw force is given by

$$F_{\mathrm{Z}} = F^1_{\mathrm{Z}} \cos(\theta) + F^1_{\mathrm{Y}} \sin(\theta) \tag{2}$$

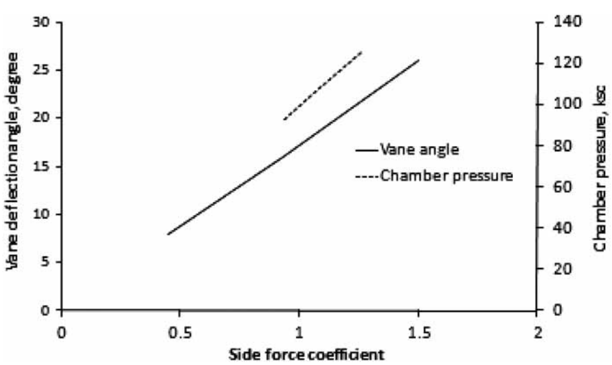

Fig. 11 Variation of side force coefficient with chamber pressure and vane angles

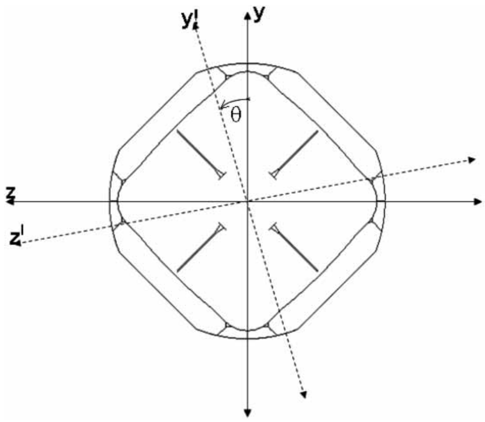

Fig. 12 Vehicle rear view showing rotational offset angle sign convention

The net pitch force is given by

$$F_{\mathrm{Y}} = F^1_{\mathrm{Y}} \cos(\theta) - F^1_{\mathrm{Z}} \sin(\theta) \tag{3}$$

The net roll moment is given by

$$R = \frac{F^1_{\mathrm{R}} r}{B} \tag{4}$$

where r is the minimum distance between the vane centre of pressure location and missile axis; $A = 23.2602$ and $B = 0.7071$ are the model constants obtained from the regression analysis. The sign convention coefficients ξ's for different force calculations are tabulated in Table 2.

The developed correlation is checked with CFD data and valid experimental data to find out the error band of the correlation. Time history of the predicted side force coefficient (both pitch and yaw force coefficients) is compared with the CFD data in Fig. 13. The correlation closely resembles the full CFD simulation. An average error of around ±2 per cent is observed between the correlation and CFD data. Therefore, the correlation can complement the CFD analysis for the prediction of yaw force, pitch force, roll moment, etc. The non-dimensionalized yaw force coefficients calculated from the correlation is compared with the experimental results in Fig. 14. The raw data of measurement have been used for comparison. The fluctuation in the measured side force is due to the vibration of the motor. The experimental uncertainty in the side force measurement is of the order of ±2 per cent. A good comparison of the predicted and experimental values is obtained. The theoretical correlation can be

Table 2 Sign computation coefficients for different force calculations

	ξ_1	ξ_2	ξ_3	ξ_4
Yaw	1	−1	−1	1
Pitch	1	1	−1	−1
Roll	1	1	1	1

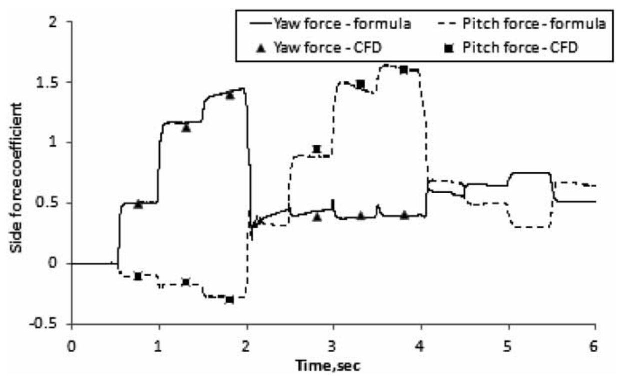

Fig. 13 Comparison of side force coefficient between the correlation and CFD data

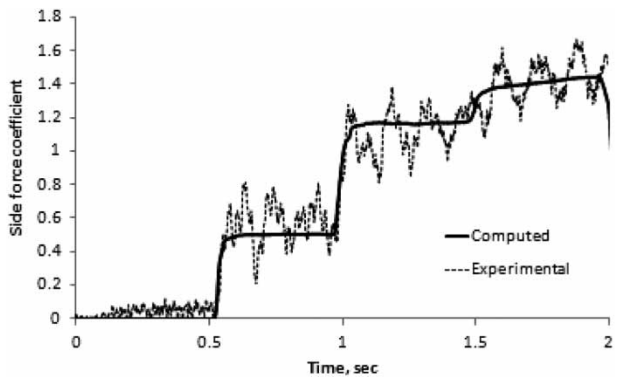

Fig. 14 Comparison of yaw force coefficient between theoretical correlation and experimental data

utilized in the On-Board Computer (OBC) to generate necessary side/roll forces on the aerospace vehicle.

5 CONCLUDING REMARKS

The flow field of a rocket nozzle with a jet vane mounted at its rear is simulated numerically using commercial CFD software. The 3D Navier–Stokes equations along with the K–ε turbulence model are solved. A hybrid grid consisting of an unstructured grid in the jet vane assembly and a multi-block structured hexahedral grid in the remaining portion of the flow field is employed. Grid independence of the results is demonstrated by simulating the flow field with three different grids and by comparing the results. Simulation captures all the essential features of the flow field including the complex compression/expansion wave interactions emanating from the vane surfaces and shrouds. The computed side force coefficients are seen to vary linearly with chamber pressure and vane deflection angles. Non-linear regression analysis is performed to develop a theoretical correlation from the CFD database to predict the force and moment coefficients for different chamber pressures, vane deflection angles, and roll offset angles. The data obtained from the correlation compare very well with full CFD simulation as well as the experimental data of the motor static test. The theoretical correlation can be utilized in the OBC to generate necessary side/roll forces on the aerospace vehicle.

REFERENCES

1 **Lyod, R.** and **Thorp, G. P.** A review of TVC system for tactical missile. AIAA paper 78-1071, 1978.
2 **Roger, R. P., Chan, S. C.,** and **Hunley, J. D.** CFD analysis for the lift and drag on a fin/moment as a jet vane TVC for boost control. AIAA paper 95-0083, 1995.
3 **Woodberry, R. F. H.** and **Zeamber, R. J.** Solid rocket thrust vector control. NASA Space Vehicle Design Criteria, NASASP-8114, 1974.
4 **Facciano, A. B.** Evolved seasparrow missile jet vane control system prototype hardware development. *J. Spacecr. Rockets*, 2002, **39**(4), 522–531.
5 **Sung, H.-G.** and **Hwang, Y.-S.** Thrust vector characteristics of jet vane arranged in X-formation within a shroud. *J. Propuls. Power*, 2004, **20**(3), 501–508.
6 **Kampa, D., Weirs, A.,** and **Schmucker, R.** Material problem in jet vane thrust vector control system. Report no. AGARD CP-259, NATO Research and Technology Organisation, 1979.
7 **Harrison, V., Dechamplain, A., Kretschmer, D., Farinaccio, R.,** and **Stowe, R. A.** Force measurements evaluating erosion effects on a jet vanes for a thrust vector control system. AIAA paper 2003-5237, 2003.
8 **Giladett, L. V.** and **Wineman, A. R.** Investigation of vanes immersed in the jet of a solid fuel rocket motor. Report no. NACA RM L 52 F 12, National Advisory Committee for Aeronautics, Washington, 1952.
9 **Rahaim, C. P., Cava Leri, R. J., McCarthy, J. G.,** and **Kasab, A. J.** Jet vane thrust vector control: a design effort. AIAA paper 96-2904, 1996.
10 **Baldwin, B. S.** and **Lomax, H.** Thin layer approximation and algebraic model for separated turbulent flows. AIAA paper 78-257, 1978.
11 **Zhang, H. S., So, R. M. C., Speziale, C. G.,** and **Lai, Y. G.** A near wall two equation model for compressible turbulent flow. AIAA paper 92-0442, 1992.
12 **Saha, S., Sinha, P. K., Sampath Kumar, K., Satyanarayana, A.,** and **Chakraborty, D.** Jet vane flowfield characteristics using CFD. In *Recent trends in aerospace design and optimization* (Eds B. Uthup, S. P. Koruthu, R. K. Sharma, and P. Priyadarshi), Proceedings of SAROD-2005, 2005, pp. 335–346 (Tata McGraw-Hill, India).
13 **Yu, M. S., Cho, H. H., Hwang, K. Y.,** and **Bac, J. C.** Numerical study on a thermal response of the jet vane system in a rocket nozzle. AIAA paper 2004-997, 2004.
14 **Yu, M. S., Cho, H. H., Hwang, K. Y.,** and **Bac, J. C.** A study on a surface ablation of the jet vane system in a rocket nozzle. AIAA paper 2004-2276, 2004.
15 **Yu, M. S., Cho, H. H., Hwang, K. Y.,** and **Bac, J. C.** Hybrid method for jet vane thermal analysis in supersonic nozzle flow. *J. Thermophys. Heat Transf.*, 2006, **20**(3), 614–617.
16 **Roe, P. L.** Characteristic based schemes for the Euler equations. *Annu. Rev. Fluid Mech.*, 1986, **18**, 337–365.

APPENDIX

Notation

A	model constant
B	model constant
C_F	force coefficient
D	nozzle exit diameter (m)
F	side force (Kgf)
P_c	chamber pressure (Ksc)
q	free stream dynamic pressure (Ksc)
r	radial distance from the centre of pressure on a jet vane to the missile axis (m)
R	roll moment (Kgf-m)
S	vehicle cross-sectional area (m^2)
δ	vane deflection angle (degree)
θ	missile rotational offset angle (degree)
ξ	constant for sign convention

Subscripts

R	roll configuration
Y	pitch configuration
Z	yaw configuration
1	vane number 1
2	vane number 2
3	vane number 3
4	vane number 4

Superscript

1	referring to offset coordinates